# Nonlinear stability analysis of the growth surface during diamond chemical vapor deposition

Pushpa Mahalingam and David S. Dandy[a)]
*Department of Chemical Engineering, Colorado State University, Fort Collins, Colorado 80523-1370*

(Received 17 October 1997; accepted for publication 6 March 1998)

The morphological stability of the solid–gas interface under conditions of diffusive transport of reactant species towards the surface during the chemical vapor deposition process is analyzed using linear and nonlinear perturbation theories. The Landau coefficient, which represents the nonlinear growth rate, is calculated using the direct method of undetermined coefficients. A dispersive relation is derived which relates the effects of species diffusive transport towards the growing interface, surface diffusion, and geometrical factors with the stability of perturbations on the interface. The resulting relation is applied to the diamond chemical vapor deposition process. Linear and nonlinear instability of the interface is obtained for diamond chemical vapor deposition conditions. Linear instability increases but the Landau coefficient becomes larger, indicating greater nonlinear stability as the reactor pressure increases, although both linear and nonlinear analyses suggest more stability as the reactor temperature increases. However, during typical diamond growth conditions, it is predicted that the diamond–gas interface is unstable to both infinitesimal and finite amplitude disturbances. © *1998 American Institute of Physics.* [S0021-8979(98)07611-7]

## I. INTRODUCTION

The onset of morphological instability in the chemical vapor deposition (CVD) process and the critical properties that cause an initially planar interface to break down have been predicted by means of linear perturbation analyses.[1–9] In general, CVD constitutes a free-boundary problem for which the interface shape and position are unknown, and therefore the temperature and concentration fields at the gas–solid interface are also unspecified. If the amplitude of the interface shape perturbation can be assumed to be infinitesimal, linear perturbation analysis may be applied to study the onset of interface instability. This approach has been adopted by a number of investigators in the study of CVD processes[1–9] and the analogous solidification problem.[10–16] Overviews of morphological linear stability analysis applied to the solidification problem are available.[17–19]

Linear stability analysis predicts critical values of the governing parameters for the onset of instability.[20] The amplitude of the perturbation imposed on the interface is infinitesimal in this case. However, a linear analysis is limited in scope to predicting only the onset of instability; it cannot be used to analyze the possible evolution of the unstable planar interface to a nonplanar cellular interface. The exponential temporal growth rate of the perturbation predicted by linear theory is not suitable for describing the actual growth of the interface due to the fact that higher-order terms in the growth rate expression are neglected—terms that are not negligible once the interface shape deviates sufficiently far from planarity. In order to study the perturbation and growth behavior of an interface more accurately over a relatively longer period of time, it is necessary to retain higher-order terms in the growth rate, requiring a nonlinear analysis.

A number of investigations have been carried out to extend beyond the linear growth regime when examining the stability of a solidification growth front,[21–30] but the study of the nonlinear stability of a solid–gas interface during a CVD process has been reported in only one instance.[31] Three types of theoretical treatment of the nonlinear problem for the directional solidification of a binary alloy can be identified in the literature. One approach, using expansion methods, provides nonplanar interface solutions where the amplitude of perturbation is finite but very small. This is a weakly nonlinear method and was adopted by Wollkind and Segal[21] using a Stuart–Watson approach[22,23] to study interface stability during the solidification of a dilute binary alloy. The Landau coefficient in the amplitude equation was calculated by means of an adjoint eigenvalue approach. Wollkind *et al.*[24] also studied the interface stability of a binary alloy using the direct method to calculate the Landau coefficient. They showed that, for the moving boundary problems under consideration, the direct method was superior to the adjoint operator method, particularly when the solution itself is desired in addition to the solvability condition.

A second approach has been to replace the full set of equations governing the system with a set of equations that are much easier to solve. These are the so-called geometrical[25] or boundary-layer models.[26] The essential feature of these models is that they approximate the temperature gradients at the interface, thereby eliminating the need to solve the equation governing energy transport. The problem is then reduced to solving a first-order nonlinear equation in one variable. The drawback to this approximation is that it ignores all global properties associated with the transport equation and at long times these models produce unphysical phenomena such as boundaries that cross. Nevertheless, this approach provides important insights into solidification processes.

[a)]Electronic mail: dandy@engr.colostate.edu

 

The third approach has been full-scale numerical evaluation of the entire set of equations governing the solidification process.[27–30] This approach avoids the problems of the approximations inherent to the two methods above, but the numerical effort required may be significant. Palmer and Gordon[31] examined the morphological stability of both one- and two-dimensional solid–gas interfaces well into the nonlinear regime during a CVD process. They developed a first-order differential equation for the motion of the interface which was then integrated numerically to determine the boundary position as a function of time.

Mahalingam and Dandy[9] employed a linear perturbation theory to analyze the interface stability during the diamond CVD process, including diffusive transport of reactive species to the interface, surface reaction kinetics, and surface diffusion. In the present study, nonlinear perturbation analysis is applied to the CVD process with the inclusion of all relevant physical processes, including reactant gas-phase diffusion, surface diffusion, and surface reaction kinetics. An expression for the Landau coefficient is derived that incorporates surface diffusion, surface reaction kinetics, and the diffusive transport of species to the interface. The linear and nonlinear results are then applied to typical diamond CVD process conditions to explore the stability of the diamond–gas interface.

## II. FORMULATION

In this work, a convective diamond CVD process such as the direct current (dc) arcjet or combustion torch is studied using a two-dimensional stability analysis. These systems typically consist of a downward stagnation flow which transports the reactant species to the top of the boundary layer by convection.[32] Within the boundary layer, the species are transported to the substrate surface primarily by diffusion. A stability analysis is applied to the boundary layer region of these convective systems. Once the species are transported to the surface, they undergo surface reactions such as H atom abstraction and termination, and adsorption of $CH_3$ on the surface.[33] A description of such a chemical vapor deposition process must therefore contain four elements: (1) mass transport to the surface, (2) incorporation of individual species onto the surface by thermally activated kinetic processes, (3) mass transport along the solid surface by surface diffusion, and (4) re-evaporation of the adsorbed species into the gas phase. A schematic of the problem domain is shown in Fig.1.

In this study, the following assumptions have been made to simplify the mathematical analyses:

(1) The gas phase consists only of $CH_3$, H, and $H_2$.

(2) The gas phase species are transported solely by diffusion in the boundary layer and deposited on the surface under isothermal conditions. It has been shown by Mahalingam and Dandy[9] that the Knudsen numbers of H in $H_2$ at pressures and temperatures typical of diamond CVD process are significantly less than unity, justifying the use of a continuum equation within the boundary layer to describe the transport of species to the gas–solid interface. The Knudsen number is defined as the ratio of the mean free path, $\lambda$, to the characteristic reactor scale, taken here to be the boundary layer thickness, $L$. The expression used to calculate $\lambda$ for a mixture is defined by Reid *et al.*[34] The boundary-layer thickness, $L$, for the stagnation flow geometry may be evaluated using the proportionality of $L$ with the gas phase temperature derived by Dandy and Yun.[35] They calculated that $L \propto P^{-1/2}$ and $L \propto T^{3/4}$, where $P$ is the total pressure in the reactor and $T$ is the gas temperature. Given a predicted value of $L=0.5$ cm for a pressure of 30 Torr and a mean gas temperature of 1800 K within the boundary layer,[33] the boundary layer thickness, $L$ can be calculated at other pressures and temperatures based on its proportionality on gas phase temperature and pressure.

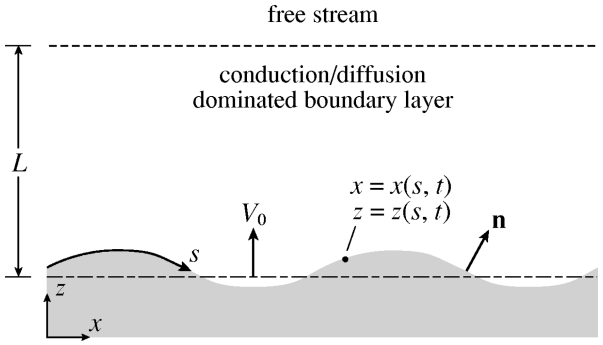


FIG. 1. Schematic of the problem domain. The diamond surface position is represented by $x(s,t), z(s,t)$, where $s$ is the arc length along the surface, $t$ is time, and **n** is the unit normal to the surface. The boundary-layer thickness is denoted by $L$.

(3) Homogeneous gas phase reactions during diffusion in the boundary layer are excluded. This assumption is reasonable because the H and $CH_3$ concentrations drop by less than an order of magnitude within the boundary layer even when gas phase reactions are considered.[33]

(4) Re-evaporation (desorption or etching) of diamond is expected to be negligible.[36]

Based on the assumptions stated above, the governing equations for the transport of H and $CH_3$ in the boundary layer are obtained from the species conservation equations, which reduce to the following form:

$$\frac{\partial C_i}{\partial t} = \mathscr{D}_i \nabla^2 C_i, \tag{1}$$

where $\mathscr{D}_i$ is the binary diffusivity of species $i$ in $H_2$, $C_i$ is the gas-phase concentration, and the subscript $i$ refers to $CH_3$ or H. Although the gas phase is a multicomponent mixture, the transport of H and $CH_3$ may be treated as binary due to the large excess of $H_2$ in the system.

The boundary condition for $CH_3$ and H at the top of the boundary layer, that is, at $z=L+V_0 t$ is given by

$$C_i = C_i^0, \tag{2}$$

where $V_0$ is the constant mean velocity of the interface, $t$ is time, and $C_i^0$ is obtained from detailed stagnation flow calculations.

Methyl radicals transported to the surface by diffusion may be adsorbed, leading to the growth of diamond films. Therefore, from a mass balance, the flux of $CH_3$ to the sur-

face must equal the net incorporation rate of that species at the surface. The boundary condition for $CH_3$ at the interface is given by

$$\mathscr{D}_{CH_3}\mathbf{n}\cdot\nabla C_{CH_3}=k_{CH_3}\frac{C^s_{CH_3}C^s_H}{b+C^s_H}, \tag{3}$$

where the superscript $s$ denotes the gas-phase concentrations of species at the surface, and the values of the parameters are taken from the literature:[37] $k_{CH_3}=1469.5$ cm/s and $b=5\times10^{-9}$ mol/cm$^3$. As illustrated in Fig. 1, $\mathbf{n}$ is the unit normal to the surface, directed into the gas phase.

Hydrogen atoms transported to the surface undergo abstraction and termination reactions. Mass conservation at the surface requires that the diffusive flux of H to the surface is equal to the surface/heterogeneous recombination rate of atomic hydrogen.[38] The boundary condition for H at the interface is therefore given by

$$\mathscr{D}_H\mathbf{n}\cdot\nabla C_H=k_H C^s_H=\frac{\gamma_H\vartheta_H}{4}C^s_H, \tag{4}$$

where $\gamma_H$ is the recombination coefficient, that is, the probability that an H atom recombines when striking the surface, $\vartheta_H$ is the mean thermal speed of an H atom given by $(8RT/\pi m_H)^{1/2}$, where $m_H$ is the molecular weight of atomic hydrogen, $R$ is the gas constant, and $T$ is the effective temperature of the gas phase, such that $T=T(_s+T_g)/2$, where $T_s$ is the temperature of the substrate, and $T_g$ is the temperature of the gas at the top of the boundary layer, $z=L$. The expression used in this work to evaluate binary diffusion of $CH_3$ and H in $H_2$ is taken from Dandy and Coltrin.[33]

Convective diamond CVD processes such as the dc arcjet or combustion torch are high growth rate techniques. The concentration of H at the growth surface, $C^s_H$, is much larger than $b$,[37,38] and consequently the boundary condition on $CH_3$ at the interface—that is, Eq. (3)—reduces to the approximate expression

$$\mathscr{D}_{CH_3}\mathbf{n}\cdot\nabla C_{CH_3}=k_{CH_3}C^s_{CH_3}. \tag{5}$$

Because the boundary condition at the interface given by Eq. (5) involves only the concentration of methyl radicals at the surface, the governing equation (1) for the transport of $CH_3$ alone may be solved to fully describe the system. Therefore, in the following the subscript $CH_3$ will be dropped from $C$ when denoting the concentration of $CH_3$.

The position of the interface, $z=\epsilon\zeta(x,t)+V_0t$, is described by $v(x,t)$, the component of the interface velocity coincident with $\mathbf{n}$. When surface diffusion is considered, the following nonlinear equation may be derived for $v$:

$$v(x,t)=\pi\mathscr{D}_{CH_3}(1+\delta\kappa)\mathbf{n}\cdot\nabla C-\beta'\nabla_s^2\kappa, \tag{6}$$

where $\epsilon\,\zeta(x,t)$ is an infinitesimal disturbance superposed on a flat interface, $\pi$ is the molar volume of diamond, $\delta$ is the length scale of a C atom ($1.0\times10^{-8}$ cm), $\nabla_s^2$ is the surface Laplacian operator, $\kappa$ is the surface curvature, and $\beta'$ is the surface diffusion term given by

$$\beta'=\frac{\mathscr{D}_s\Omega^2\theta\psi}{k_BT_s}. \tag{7}$$

In this expression $\Omega$ is the molecular volume of diamond, $\theta$ is the surface tension, $\mathscr{D}_s$ is the surface diffusion coefficient of carbon atoms on diamond, $\psi$ is the number of atoms per unit area of diamond surface, and $k_B$ is Boltzmann's constant. The curvature term in Eq. (6) represents a geometrical effect, also included in the Kardar–Parisi–Zhang equation.[39] The surface diffusion term present in Eq. (7) is similar to the ones derived by Mullins[40] and Muller.[41]

For an interface of the form presented in Fig. 1, $\mathbf{n}$ and $v(x,t)$, are given by[21]

$$\mathbf{n}=\frac{(-\epsilon\zeta_x,1)}{\sqrt{1+\epsilon^2\zeta_x^2}} \tag{8}$$

and

$$v(x,t)=\frac{V_0+\epsilon\zeta_t}{\sqrt{1+\epsilon^2\zeta_x^2}}, \tag{9}$$

where the subscripts $x$ and $t$ denote derivatives with respect to these variables. The curvature $\kappa$ and the surface Laplacian $\nabla_s^2$ in Eq. (6) are given by[21]

$$\kappa=\frac{\epsilon\zeta_{xx}}{(1+\epsilon^2\zeta_x^2)^{3/2}} \tag{10}$$

and

$$\nabla_s^2=\frac{1}{1+\epsilon^2\zeta_x^2}\frac{\partial^2}{\partial x^2}-\frac{\epsilon^2\zeta_x\zeta_{xx}}{(1+\epsilon^2\zeta_x^2)^2}\frac{\partial}{\partial x}. \tag{11}$$

A coordinate system is introduced that moves along with the interface at speed $V_0$:

$$z=\bar{z}-V_0t. \tag{12}$$

After nondimensionalization with a characteristic length scale $l_c=L$, concentration scale $C_c=C^0_{CH_3}$, and time scale $t_c=L/V_0$, and subsequent transformation to the new coordinate system, the governing Eq. (1) becomes

$$\frac{\partial C}{\partial t}=\frac{\partial C}{\partial z}+\frac{1}{\mathrm{Pe}}\left(\frac{\partial^2C}{\partial x^2}+\frac{\partial^2C}{\partial z^2}\right), \tag{13}$$

where the Peclet number is $\mathrm{Pe}=LV_0/\mathscr{D}_{CH_3}$. In diamond CVD the Peclet number inside the boundary layer varies from $10^{-11}$ to $10^{-7}$, depending on the processing conditions; generally, Pe has a positive correlation with the growth rate that may be achieved in a device. The boundary condition (2) at the top of the boundary layer, $z=1$, then becomes

$$C=1, \tag{14}$$

and boundary condition (5) at the interface, $z=\epsilon\zeta(x,t)$, becomes

$$\frac{1}{\mathrm{Pe}}\left(-\epsilon\zeta_x\frac{\partial C}{\partial x}+\frac{\partial C}{\partial z}\right)=\xi C, \tag{15}$$

where $\xi=k_{CH_3}/V_0$.

The position of the interface [Eq. (6)], $z=\epsilon\zeta(x,t)$, is nondimensionalized to give

$$\epsilon\zeta_t=\rho \mathrm{Pe}^{-1}(1-\delta\kappa)\left(-\epsilon\zeta_x\frac{\partial C}{\partial x}+\frac{\partial C}{\partial z}\right)$$
$$-\beta\sqrt{1+\epsilon^2\zeta_x^2}(\nabla_s^2\kappa)-1, \tag{16}$$

where $\rho=\bar{\omega}C^0_{\mathrm{CH}_3}$ and $\beta=\beta'/L^3V_0$.

The governing Eq. (13) along with boundary conditions (14) and (15), and the interface position Eq. (16) are applied to the stability analysis.

## III. SOLUTION PROCEDURE

In order to study the nonlinear morphological stability of the diamond growth interface, a perturbation approach is adopted using the following steps:[11,12] (i) obtain an analytical steady state solution for the unperturbed planar interface; (ii) impose an arbitrary finite amplitude disturbance on the initially planar interface, small enough that all terms of order higher than $3(\epsilon>3)$ can be neglected (nonlinear perturbation analysis); (iii) obtain an approximate solution for the case of the perturbed interface using perturbation theory; and (iv) examine the solution and determine whether the interface perturbation will grow with time (unstable) or decay (stable).

### A. Steady state solution for planar interface

Following the procedure outlined above, the steady state solution to Eq. (13) is found, subject to its boundary conditions: Eq. (14) at the top of the boundary layer ( $z=1$) and Eqs. (15) and (16) at the interface ($z=0$), assuming the interface to be planar. The corresponding steady state planar solution is

$$C_0(z)=A+Be^{-\mathrm{Pe}\,z}, \tag{17}$$

where $A=(1+\xi)/(1+\xi-\xi e^{-\mathrm{Pe}})$ and $B=-\xi/(1+\xi-\xi e^{-\mathrm{Pe}})$. The mean velocity of the interface, $V_0$, is defined uniquely by

$$e^{-\mathrm{Pe}}-(1+\xi)/\xi+\rho=0. \tag{18}$$

### B. Perturbing the interface

A perturbation $z=\epsilon\zeta(x,t)$ is imposed on the initially planar interface. The amplitude function $\zeta(x,t)$can be written in terms of $\epsilon$ so that

$$z=\epsilon\zeta(x,t)=\sum_{n=1}^{\infty}\epsilon^n\zeta_n(x,t). \tag{19}$$

For the weakly nonlinear analysis considered in this work, it is assumed that the perturbation amplitude is finite but small enough that all the terms of higher order greater than 3 can be neglected. Therefore,

$$z=\epsilon\zeta(x,t;\epsilon)=\epsilon\zeta_1(x,t)+\epsilon^2\zeta_2(x,t)+\epsilon^3\zeta_3(x,t). \tag{20}$$

Once the interface is perturbed the corresponding gas phase concentration field will also be perturbed. Thus,

$$g(x,z,t;\epsilon)=g_0(z)+\sum_{n=1}^{3}\epsilon^n g_n(x,z,t), \tag{21}$$

where

$$g(x,z,t;\epsilon)=[C(x,z,t;\epsilon),\ \epsilon\zeta(x,t;\epsilon)]^T. \tag{22}$$

According to the Fourier theory,[10,11] an infinitesimal perturbation can be built up in terms of $x$ as a superposition of sinusoidal waves with an arbitrary frequency $\omega$:

$$z=\epsilon\zeta_1(x,t)=\epsilon\zeta_{11}e^{a_0t}\cos\,\omega x, \tag{23}$$

when all higher-order terms in $\epsilon$ are neglected and only the first-order term is retained. In Eq. (23) $\zeta_{11}$ is a constant, and $a_0$ is the linear growth rate satisfying

$$\frac{1}{\epsilon\zeta_1}\frac{\partial}{\partial t}(\epsilon\zeta_1)=a_0. \tag{24}$$

In order for the above solutions to satisfy the boundary conditions at the interface,

$$g_0(z)=[C_0(z),0]^T, \tag{25}$$

$$g_1(x,z,t)=A(t)g_{11}(z)\cos\,\omega x, \tag{26}$$

$$g_2(x,z,t)=A^2(t)[g_{20}(z)+g_{22}(z)\cos 2\omega x], \tag{27}$$

$$g_3(x,z,t)=A^3(t)[g_{31}(z)\cos\,\omega x+g_{33}(z)\cos 3\omega x], \tag{28}$$

where the spatial and time dependence of the quantities $g_n$ ($n=1,\ 2,\ 3$) are to be determined,[21,42] $A(t)$ is an unknown amplitude associated with interface growth rate, and $g_{ij}(z)=[C_{ij}(z),\ \epsilon\zeta_{ij}]^T$. The growth rate of the interface, $d[\epsilon A(t)]/dt$, satisfies

$$\epsilon\frac{dA(t)}{dt}\equiv\epsilon\dot{A}(t)=a_0\epsilon A(t)-a_1\epsilon^3A^3(t), \tag{29}$$

where $a_0$ is the linear growth rate and $a_1$ is the third-order growth rate, usually referred to as the Landau coefficient.

### C. Linear perturbation analysis

For the linear perturbation analysis, the imposed perturbation is assumed to have an infinitesimal amplitude, such that only the first-order term in Eq. (21) needs to be retained and Eqs. (23) and (24) result. The approximate solution for the concentration field should have a form similar to the perturbation at the interface, that is,

$$C(x,z,t;\epsilon)=C_0(z)+\epsilon C_{11}(z)e^{a_0t}\cos\,\omega x. \tag{30}$$

Expressions (23) and (30) are substituted into the governing Eq. (13) and the corresponding boundary conditions at the top of the boundary layer Eq. (14), and at the interface, Eqs. (15) and (16). Taylor series is used to expand the boundary conditions at the interface about $z=0$. Retaining only the terms of the first order in $\epsilon$ and neglecting all higher-order terms, one obtains from the governing equation (13) and boundary conditions (14) and (15)

$$[\mathrm{Pe}^{-1}D^2+D-(\mathrm{Pe}^{-1}\omega^2+a_0)]C_{11}(z)=0, \tag{31a}$$

$$C_{11}(1)=0, \tag{31b}$$

$$\mathrm{Pe}^{-1}DC_{11}(0)-\xi C_{11}(0)+Q_{11}\zeta_{11}=0, \tag{31c}$$

where the differential operator is $D\equiv d/dz$, and $Q_{11}=(1+\xi)B\ \mathrm{Pe}$. On solving Eqs. (31) an expression for $C_{11}(z)$ is obtained:

$$C_{11}(z)=A_{11}e^{\omega_{11}z}+B_{11}e^{\omega^*_{11}z}, \tag{32}$$

where

$$\omega_{11},\omega_{11}^{*}=-\tfrac{1}{2}\ \mathrm{Pe}\pm\sqrt{\mathrm{Pe}^2/4+\omega^2+\mathrm{Pe}\,a_0},$$
$$B_{11}=-Q_{11}\zeta_{11}/D_{11},\qquad A_{11}=-\mu_{11}B_{11},$$
$$\mu_{11}=\exp(\omega_{11}^{*}-\omega_{11}),\tag{33}$$

and

$$D_{11}=\mathrm{Pe}^{-1}(\omega_{11}^{*}-\mu_{11}\omega_{11})-\xi(1-\mu_{11}).$$

Equation (16) is expanded using Taylor series about $z=0$ to obtain

$$a_0\zeta_{11}=\rho\mathrm{Pe}^{-1}[B\mathrm{Pe}^2\zeta_{11}+DC_{11}(0)-B\mathrm{Pe}\delta\omega^2\zeta_{11}]-\beta\omega^4\zeta_{11}.\tag{34}$$

On substituting Eq. (32) into Eq. (34), an expression for the linear growth rate $a_0$ is found:

$$a_0=B\rho(\mathrm{Pe}-\delta\omega^2)+Q_{11}\rho(\mu_{11}\omega_{11}-\omega_{11}^{*})/(\mathrm{Pe}\,D_{11})-\beta\omega^4.\tag{35}$$

Equation (35) is similar to the dispersion relations derived by Viljoen.[7]

### D. Nonlinear perturbation analysis

In Sec. III, the stability of the planar interface solution of the basic Eqs. (13)–(16) to the linearized perturbation equations (infinitesimal disturbances) is examined. In this section, the stability of the planar interface solution to finite amplitude disturbances satisfying the full nonlinear perturbation equations is investigated. Equations (21)–(28) are substituted into the governing equation and boundary conditions (13)–(16), and the interface boundary conditions are expanded in a Taylor series about $z=0$ and then required to satisfy Eqs. (13)–(16) for each order of $\epsilon$. Algebraic manipulations then yield systems of linear ordinary differential equations for each order of $\epsilon$.

The formulation and solution of the $O(\epsilon)$problem has already been derived and is reported in the linear perturbation analysis section. The eigenvalue $a_0$ is given by Eq. (35). The $O(\epsilon^2)$ and $O(\epsilon^3)$ problems are similar to the $O(\epsilon)$ problem and are presented below.

#### 1. The $O(\epsilon^2)$ problem

Two sets of equations result from Eqs. (13)–(16), one with terms involving $\epsilon^2A^2(t)$ and the other $\epsilon^2A^2(t)\cos\omega x$. Upon canceling the common factor $\epsilon^2A^2(t)$, the governing Eq. (13) and boundary conditions (14) and (15) become

$$(\mathrm{Pe}^{-1}D^2+D-2a_0)C_{20}(z)=0,\tag{36a}$$

$$C_2(1)=0,\tag{36b}$$

$$\mathrm{Pe}^{-1}DC_{20}(0)-\xi C_{20}(0)+Q_{20}\zeta_{20}=R_{20},\tag{36c}$$

where $D$ is the differential operator $d/dz$, $Q_{20}=(1+\xi)B\mathrm{Pe}$, and the factor $R_{20}$ is presented in the Appendix. On solving Eqs. (36) the following solution is obtained for $C_{20}(z)$:

$$C_{20}(z)=A_{20}e^{\omega_{20}z}+B_{20}e^{\omega_{20}^{*}z},\tag{37}$$

where

$$\omega_{20},\omega_{20}^{*}=-\tfrac{1}{2}\mathrm{Pe}\pm\sqrt{\mathrm{Pe}^2/4+2a_0\mathrm{Pe}},$$
$$B_{20}=-P_{20}/D_{20},\qquad A_{20}=-\mu_{20}B_{20},\tag{38}$$
$$\mu_{20}=\exp(\omega_{20}^{*}-\omega_{20}),\qquad P_{20}=Q_{20}\zeta_{20}-R_{20},$$

and

$$D_{20}=\mathrm{Pe}^{-1}(\omega_{20}^{*}-\omega_{20}\mu_{20})-\xi(1-\mu_{20}).$$

To determine $C_{20}$, $\zeta_{20}$ must to be evaluated, and this quantity is obtained by expanding Eq. (16) about $z=0$ to obtain $\zeta_{20}=S_{20}/N_{20}$, where $S_{20}$ and $N_{20}$ are given in the Appendix.

Next, upon canceling $\epsilon^2A^2(t)\cos 2\omega x$ from the governing Eq. (13) and the boundary conditions (14) and (15), the following system of equations is obtained:

$$[\mathrm{Pe}^{-1}D^2+D-(4\mathrm{Pe}^{-1}\omega^2+2a_0)]C_{22}(z)=0,\tag{39a}$$

$$C_{22}(1)=0,\tag{39b}$$

$$\mathrm{Pe}^{-1}DC_{22}(0)-\xi C_{22}(0)+Q_{22}\zeta_{22}=R_{22},\tag{39c}$$

where $D$ is the differential operator, $Q_{22}=(1+\xi)B\mathrm{Pe}$, and $R_{22}$ is presented in the Appendix. The solution to Eqs. (39) is

$$C_{22}(z)=A_{22}e^{\omega_{22}z}+B_{22}e^{\omega_{22}^{*}z},\tag{40}$$

where

$$\omega_{22},\omega_{22}^{*}=-\tfrac{1}{2}\mathrm{Pe}\pm\sqrt{\mathrm{Pe}^2/4+(4\omega^2+2a_0\mathrm{Pe})},$$
$$B_{22}=-P_{22}/D_{22},\qquad A_{22}=-\mu_{22}B_{22},\tag{41}$$
$$\mu_{22}=\exp(\omega_{22}^{*}-\omega_{22}),\qquad P_{22}=Q_{22}\zeta_{22}-R_{22},$$

and

$$D_{22}=\mathrm{Pe}^{-1}(\omega_{22}^{*}-\omega_{22}\mu_{22})-\xi(1-\mu_{22}).$$

To determine $C_{22}$, $\zeta_{22}$ must first be found and this quantity is evaluated by expanding Eq. (16) at the interface about $z=0$ to yield $\zeta_{22}=S_{22}/N_{22}$, where $S_{22}$ and $N_{22}$ are given in the Appendix.

#### 2. The $O(\epsilon^3)$ problem

Again, two sets of equations result from Eqs. (13)–(16), one with terms involving $\epsilon^3A^3(t)\cos\omega x$ and the other $\epsilon^3A^3(t)\cos 3\omega x$. Upon canceling the factor $\epsilon^3A^3(t)\cos\omega x$ from Eqs. (13)–(16), the following system of equations are obtained for $g_{31}(z)$:

$$\mathrm{Pe}^{-1}D^2C_{31}+DC_{31}-(3a_0+\mathrm{Pe}^{-1}\omega^2)C_{31}=-a_1C_{11},\tag{42a}$$

$$C_{31}(1)=0,\tag{42b}$$

$$\mathrm{Pe}^{-1}DC_{31}(0)-\xi C_{31}(0)+Q_{31}\zeta_{31}=R_{31},\tag{42c}$$

$$\rho\mathrm{Pe}^{-1}DC_{31}(0)+[\rho B(\mathrm{Pe}-\delta\omega^2)-\beta\omega^4-3a_0]\zeta_{31}+a_1\zeta_{11}=S_{31},\tag{42d}$$

respectively, where $Q_{31}=(1+\xi)\ B\mathrm{Pe}$, and $R_{31}$ and $S_{31}$ are presented in the Appendix.

There are two methods which can be used to solve for the Landau coefficient $a_1$ and thus obtain $C_{31}(z)$ and $\zeta_{31}$. One is the direct method using undetermined coefficients,[43] while the other method uses the adjoint problem of the $O(\epsilon)$ system.[21] In the present work the more straightforward direct method is used to solve the third-order system.[24] Solving

Eqs. (42) for $C_{31}(z;a_0)$ by the method of undetermined coefficients, the following resulting equations are obtained:

$$C_{31}(z;a_0)=\frac{C_{31}(0;a_0)(e^{\omega_{31}^* z}-\mu_{31}e^{\omega_{31}z})}{(1-\mu_{31})}+\frac{a_1}{2a_0}(A_{11}e^{\omega_{11}z}+B_{11}e^{\omega_{11}^* z})-\frac{a_1}{2a_0}\left(\frac{(A_{11}+B_{11})(e^{\omega_{31}^* z}-\mu_{31}e^{\omega_{31}z})}{(1-\mu_{31})}\right) \tag{43a}$$

for $a_0\neq 0$ and

$$C_{31}(z;0)=\frac{C_{31}(0;0)(e^{\omega_{11}^* z}-\mu_{11}e^{\omega_{11}z})}{(1-\mu_{11})}+\frac{B_{11}a_1\mathrm{Pe}[e^{\omega_{11}z}(-2\mu_{11}+\mu_{11}z-\mu_{11}^2 z)]}{2(1-\mu_{11})\sqrt{\mathrm{Pe}^2/4+\omega^2}}+\frac{B_{11}a_1\mathrm{Pe}[e^{\omega_{11}^* z}(2\mu_{11}+z-\mu_{11}z)]}{2(1-\mu_{11})\sqrt{\mathrm{Pe}^2/4}+\omega^2} \tag{43b}$$

for $a_0=0$, where

$$\omega_{31},\omega_{31}^*=-\tfrac{1}{2}\mathrm{Pe}\pm\sqrt{\mathrm{Pe}^2/4+\omega^2+3a_0\mathrm{Pe}} \tag{44}$$

and $\mu_{31}=\exp(\omega_{31}^*-\omega_{31})$. The function $C_{31}(z;0)$ is continuous when $a_0=0$ provided that $C_{31}(0;0)$ is continuous. Further, $DC_{31}(0;a_0)$ and $DC_{31}(0;0)$ are given by the following relations:

$$DC_{31}(0;a_0)=\frac{C_{31}(0;a_0)(\omega_{31}^*-\mu_{31}\omega_{31})}{(1-\mu_{31})}+\frac{a_1}{2a_0}\left(A_{11}\omega_{11}+B_{11}\omega_{11}^*-\left(\frac{A_{11}+B_{11}}{1-\mu_{31}}\right)(\omega_{31}^*-\mu_{31}\omega_{31})\right) \tag{45a}$$

and

$$DC_{31}(0;0)=\frac{C_{31}(0;0)(\omega_{11}^*-\mu_{11}\omega_{11})}{(1-\mu_{11})}+\frac{a_1B_{11}\mathrm{Pe}}{2(1-\mu_{11})\sqrt{\mathrm{Pe}^2/4+\omega^2}}(1+2\mu_{11}\omega_{11}^*-\mu_{11}^2-2\mu_{11}\omega_{11}), \tag{45b}$$

respectively. It may be concluded that $DC_{31}(0;0)$ is continuous when $a_0=0$ as well since $\mu_{11}$ is well behaved at that limit. The following result is therefore obtained for the Landau constant, $a_1$, in the limit $a_0\to 0$:

$$a_1=\frac{R_{31}'-S_{31}'\left(\frac{1}{\rho}-\frac{\xi\mathrm{Pe}}{\rho p_1'}\right)}{\left[\frac{p_2'}{\mathrm{Pe}}-\left(\frac{\rho p_2'}{\mathrm{Pe}}+1\right)\left(\frac{1}{\rho}-\frac{\xi\mathrm{Pe}}{\rho p_1'}\right)\right]}, \tag{46}$$

TABLE I. Stability chart for the linear and nonlinear analyses.

| $a_0<0$ (Linear stability) | | $a_0>0$ (Linear instability) | |
|---|---|---|---|
| $a_1<0$ | $a_1>0$ | $a_1<0$ | $a_1>0$ |
| Subcritical instability | Nonlinear stability | Nonlinear instability | Equilibrium stability |

where the primed quantities are evaluated in the limit as $a_0\to 0$, and

$$p_1'=\frac{\omega_{11}^*-\mu_{11}\omega_{11}}{1-\mu_{11}},$$

$$p_2'=\frac{B_{11}\mathrm{Pe}}{2(1-\mu_{11})\sqrt{\mathrm{Pe}^2/4+\omega^2}}\times(1+2\mu_{11}\omega_{11}^*-\mu_{11}^2-2\mu_{11}\omega_{11}).$$

It is instructive to note that applying the direct method with $a_0=0$ from the outset is probably the simplest way to compute the Landau-type constants.[24]

Once $a_1$ is calculated $C_{31}(z)$ may then be determined. The growth rate of the disturbance amplitude for the nonlinear case is a function of both $a_0$ and $a_1$, as can be seen in Eq. (29). In order to determine whether the interface will be stable to a finite/infinitesimal amplitude perturbation, the behavior of $A(t)$ is observed as $t\to\infty$. Four cases exist based on different signs of $a_0$ and $a_1$, and these are listed in Table I.

To investigate the diamond growth interface stability, several calculations were performed for different reactor temperatures, and pressures; first, calculations were carried out for different reactor temperatures at a constant pressure to examine the effect of temperature on morphological stability of films. Then, calculations were conducted at different reactor pressures with a constant temperature to explore the effect of pressure on the uniformity of the deposited diamond film. The four different values of pressure used in this work are 5, 30, 60, and 760 Torr, and four gas temperatures employed in the computations are 800, 1200, 1800, and 2300 K. The values of pressure and temperature used in this work are typical of the range used during diamond CVD.

## IV. RESULTS AND DISCUSSION

A number of calculations were performed to examine the effects of system variables such as reactor temperature and reactor pressure on the morphology of the deposition layer. The results are categorized based on the variation of the system variables, namely gas temperature and pressure.

First, the linear stability factor, $a_0$, is plotted in Figs. 2(a)–2(d) as a function of effective gas-phase temperature for various dimensionless disturbance wave numbers, at constant pressures of 5, 30, 60, and 760 Torr, respectively. The mole fraction of $CH_3$ at the top of the boundary layer is taken to be 0.0015 in Figs. 2(a)–2(d); this value is used since it is a typical value predicted for $CH_3$ at the top of the bound-

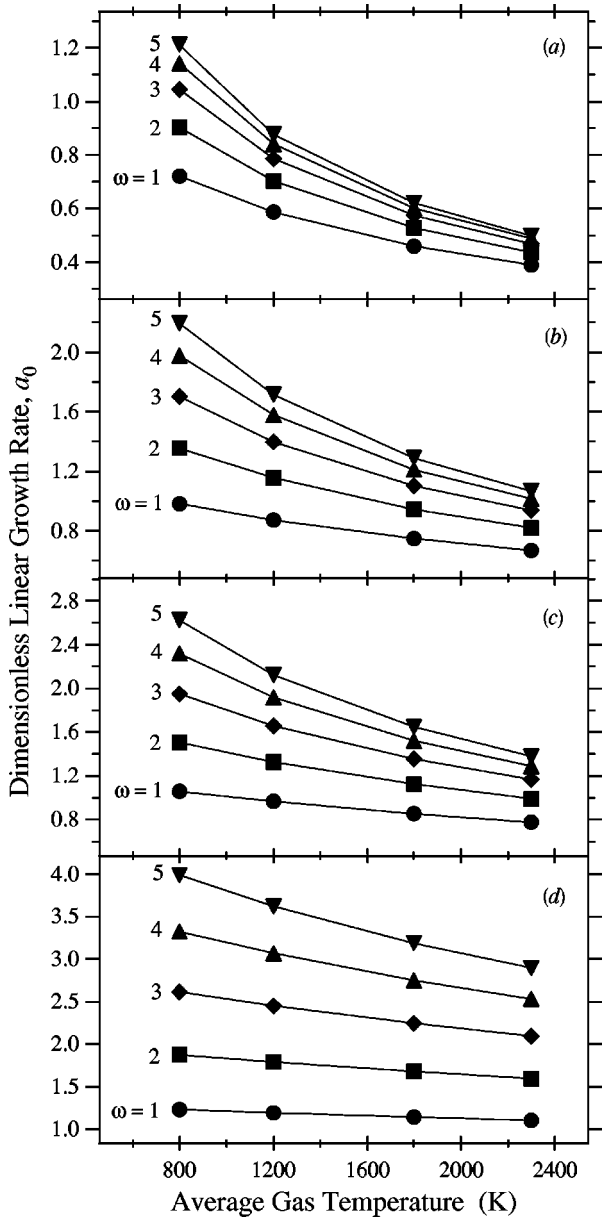


FIG. 2. The dimensionless linear growth rate, $a_0$, as a function of effective gas temperature for different values of the disturbance wavenumber, at a pressure of (a) 5 Torr, (b) 30 Torr, (c) 60 Torr, and (d) 760 Torr.

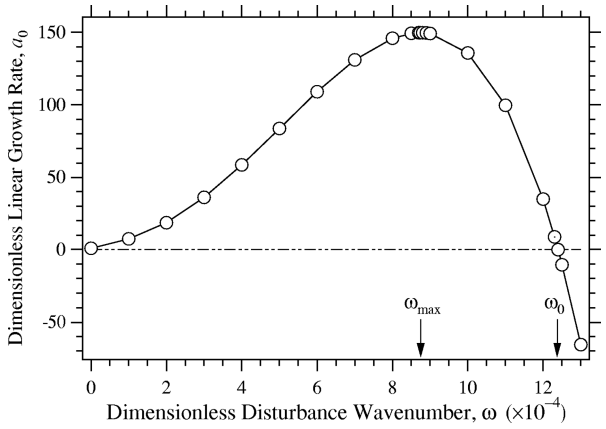


FIG. 3. The dimensionless linear growth rate, $a_0$, as a function of the dimensionless disturbance wave number, $\omega$, at a gas temperature of 1200 K, pressure of 60 Torr, and $CH_3$ mole fraction at the top of the boundary layer of 0.0015.

ary layer during diamond CVD in highly convective systems.[9] As is evident from Fig. 2(a)–2(d), $a_0$ is positive and increases with increasing pressure and decreasing temperature, indicating increasing linear instability. Even in highly convective diamond deposition systems such as those considered here, diamond growth is mass transfer limited.[9,33] Although the gas is transported rapidly by convection to the top of the boundary layer, species such as H and $CH_3$ must still diffuse through this layer to the surface. A measure of this transport rate is the Damköhler number, Da, which is the ratio of the time scale of mass diffusion through the boundary layer to the time scale characteristic of the surface reaction kinetics. This parameter may be much greater than unity even in highly convective diamond CVD systems such as dc arcjet or combustion torch.[33] The mass diffusion limitation increases with increasing pressure and decreasing temperature, and $a_0$ increases as a result. Due to the faster surface kinetics compared to reactants' diffusion and nearly negligible surface diffusion of species on the diamond growth interface,[9] the reactant species do not have time to rearrange or move about on the surface before they are incorporated into the diamond lattice, and this results in morphological instability. The effect of surface diffusion on the stability is represented by the term $-\beta\omega^4$ in Eq. (35). The term has a very strong stabilizing effect on the high wave number (that is, short wavelength) disturbances, becoming dominant as $\omega\rightarrow\infty$, but its effect is negligible for small wave number disturbances. A plot of $a_0$ versus the dimensionless disturbance wave number $\omega$ is shown in Fig. 3 for an effective gas temperature of 1200 K, pressure of 60 Torr, and a $CH_3$ mole fraction of 0.0015 at the top of the boundary layer. It can be seen from Fig. 3 that there exists a most unstable wave number, $\omega_{max}$ ($\omega_{max}=8.74\times10^4$ in Fig. 3), at which $a_0$ will have a maximum value for a given pressure and temperature, and a wave number, $\omega_0$ ($\omega_0=1.24\times10^5$ in Fig. 3), at which $a_0=0$, as shown in Fig. 3. As indicated in Fig. 3, for the conditions considered here $a_0>0$ for all $\omega<\omega_0$, $a_0=0$ at $\omega=\omega_0$, and $a_0<0$ for all $\omega>\omega_0$. Increasing the wave number of the disturbance at constant pressure and temperature increases linear instability at wave numbers less than $\omega_{max}$, as shown in Figs. 2(a)–2(d). Therefore it may be concluded that, when the process is mass transfer limited, the disturbance becomes more unstable as: (a) pressure increases for constant temperature and wave number, (b) effective gas temperature decreases at constant pressure and wave number, and (c) wave number increases at constant pressure and temperature, provided that $\omega<\omega_{max}$.

To investigate neutral stability, $a_0$ is set to zero in Eq. (35). The characteristic velocity ($V_0$), and the characteristic concentration of $CH_3$ species at the top of the boundary layer ($C_c$), are determined using Eqs. (18) and (35) for specific values of the perturbation wave number for the condition $a_0=0$; as illustrated schematically in Fig. 4, the neutral stability condition is achieved when $C_c$ has an absolute minimum at $\omega=\omega_c$. This concentration is called the critical concentration, $C_{crit}$, and the corresponding interface velocity is

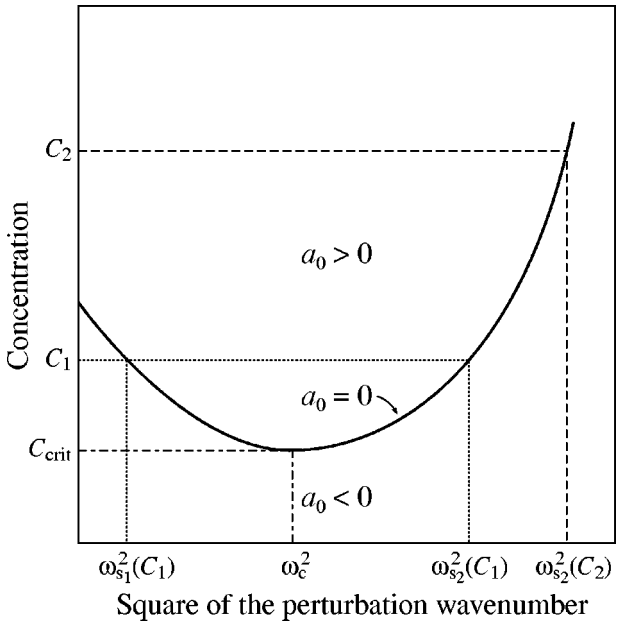


FIG. 4. A schematic plot of the concentration ($C$) as a function of the square of the perturbation wave number ($\omega^2$). The solid line represents the curve of marginal stability, for which $a_0=0$. The minimum in the marginal stability curve, $C_{crit}$, is the point of neutral stability.

called the critical velocity, $V_{crit}$. The critical velocity, critical concentration, and $\omega_c$ are then used to calculate the Landau coefficient, $a_1$, using Eq. (46). Note that the solutions obtained for $V_0$ and $C_c$ when $a_0=0$ are unique for a particular value of $\omega$.

In the plot of $C_c$ vs $\omega^2$ shown in Fig. 4, the neutral curve, or curve of marginal stability of Eq. (35) on which $a_0=0$, separates the region of instability ($a_0>0$) from that of stability ($a_0<0$).It may be seen in Fig. 4 that for $C<C_{crit}$, there exist no wave numbers, $\omega$, such that $a_0>0$, and that for $C>C_{crit}$, there exists a band of wave numbers corresponding to growing disturbances. This means that for $C>C_{crit}$ the system is unstable for a band of wave numbers ($\omega_{s1}-\omega_{s2}$) and for $C<C_{crit}$, the system is stable. Note that for a concentration $C_2$, the system is unstable for all $\omega<\omega_{s2}$. The concentration of $CH_3$ at the top of the boundary layer during a typical diamond CVD process is usually much greater than

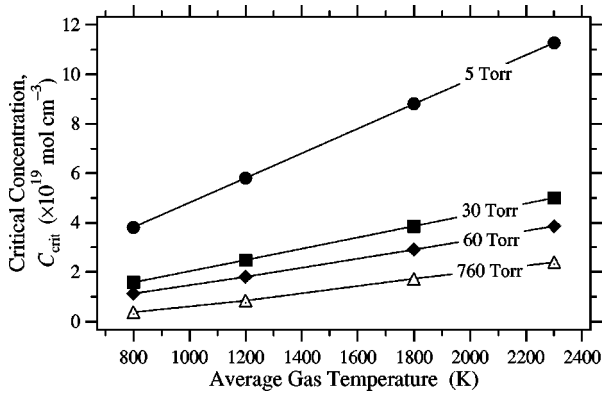


FIG. 5. The critical concentration, $C_{crit}$, as a function of the effective gas temperature at different values of pressure.

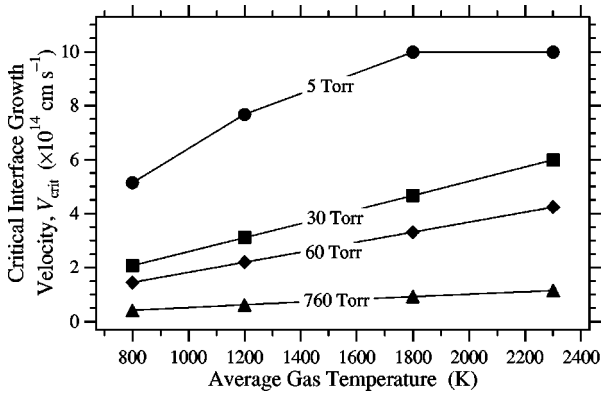


FIG. 6. The critical velocity, $V_{crit}$, as a function of the effective gas temperature at system pressures of 5, 30, 60, and 760 Torr.

the critical concentration for typical diamond CVD conditions and are such that $a_0>0$ for $\omega<\omega_{s2}$ since $\omega_{s1}=0$ at the diamond growth reactor pressures and temperatures considered in this work. The dimensionless values of $\omega_{s2}$ for the temperature and pressure used in this work are in the range $10^4$–$10^6$.

To analyze the stability of the planar interface solution to finite amplitude perturbations the signs of $a_0$ and $a_1$ in the amplitude equation must be determined. It has already been shown that $a_0>0$ for $C>C_{crit}$ and $\omega<\omega_{s2}$, $a_0=0$ if $C$ is such that it lies on the marginal stability curve, and $a_0<0$ for $C<C_{crit}$. The sign of $a_1$ will be determined by Eq. (46). In this equation it is clear that $a_1$ is a function of $\omega_c$, $V_{crit}$, and $C_{crit}$. The Landau constant, $a_1$, is then calculated from the critical parameters. A plot of $C_{crit}$, $V_{crit}$, and $\omega_c$ as functions of effective gas temperature for various values of pressure are given in Figs. 5, 6, and 7, respectively.

### A. Effect of reactor pressure

Four sets of calculations at pressures 5, 30, 60, and 760 Torr were performed for each of the effective gas temperature values 800, 1200, 1800, and 2300 K. As is evident from Fig. 5, the critical concentration, $C_{crit}$, beyond which $a_0>0$ for $\omega<\omega_{s2}$, decreases with increasing pressure. Since the critical concentration, $C_{crit}$, is much less than the concentration of $CH_3$ at the top of the boundary layer, the mag-

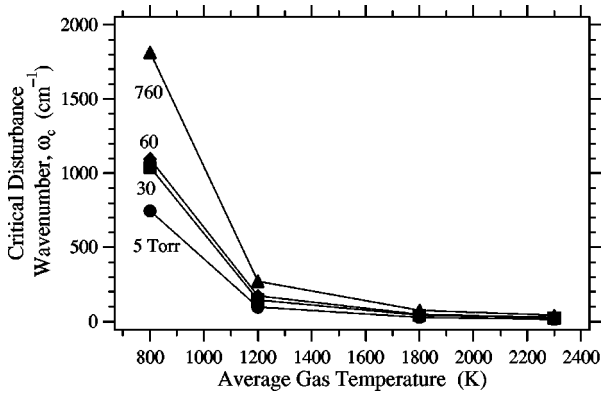


FIG. 7. The critical wave number, $\omega_c$, as a function of the effective gas temperature at system pressures of 5, 30, 60, and 760 Torr.

nitude of positive $a_0$ will increase with increasing pressure, indicating more linear instability to infinitesimal disturbances, provided the wave number of the disturbance is less than $\omega_{s2}$. From Figs. 6, and 7, it is clear that the critical velocity, $V_{\text{crit}}$, decreases with increasing pressure at constant temperature, and critical wave number $\omega_c$ increases with increasing pressure at constant temperature.

It is clear from the model formulation that the dynamic behavior of the diamond growth interface depends on the magnitudes of the reactants' gas-phase diffusivity, surface kinetics, and surface diffusion. Surface diffusion, with a magnitude characterized by $\beta$, is the interface stabilizing factor. The terms containing the Peclet number, Pe, which is a function of gas-phase diffusivity, have a positive sign in the linear stability equation for $a_0$, Eq. (35). Thus, as gas-phase diffusivity decreases (greater mass transfer limitation) with increasing pressure and/or decreasing temperature, the greater the instability in the diamond interface. As discussed earlier, even highly convective diamond CVD processes can be mass transfer limited within the boundary layer because the Damköhler number is greater than unity for important species such as H and $CH_3$. For constant temperature and increasing pressure, $\beta$ increases, suggesting higher interface stability. Also, at higher pressures Pe is larger, indicating lower gas-phase diffusivity which has a destabilizing effect on the interface stability. Therefore, for diamond deposition the value of $a_0$ increases with pressure, resulting in greater instability despite the increased $\beta$ values. This may be due to a more profound effect of the lower gas-phase diffusivity than increased $\beta$ values on $a_0$.

The value of the Landau coefficient, $a_1$, increases with increasing pressure, although its sign is negative for pressures of 5, 30 and 60 Torr. At 760 Torr, $a_1$ is positive and this is indicated by the open symbols in Fig. 5. Such a trend for $a_1$ implies that the nonlinear analysis predicts greater stability to finite amplitude disturbances with an increase in pressure. The Landau coefficient, $a_1$, increases with increasing pressures, because the effect of the increase in the stabilizing factor, $\beta$, is more pronounced in the expression for $a_1$ than in the expression for $a_0$.

Therefore, it may be concluded that the diamond interface is morphologically unstable for both infinitesimal and finite amplitude disturbances at pressures of 5, 30, and 60 Torr. The diamond interface will only be stable to finite amplitude disturbances at a pressure of 760 Torr although the linear instability to infinitesimal disturbances is greater at 760 Torr than at lower pressures because $a_0$ is more positive at higher pressures than at lower pressures. The plot of the interface velocity, $V_0$, as a function of temperature at different pressures (Fig. 8) indicates that diamond has a higher growth rate at higher pressures.

### B. Effect of temperature

It may be seen in Fig. 5 that $C_{\text{crit}}$ increases with increasing temperature, and as a result the magnitude of the instability decreases because of the decrease in $a_0$ with increasing temperature. However, for these conditions all values of $a_0$ are positive so that the effect of temperature on $C_{\text{crit}}$ is the

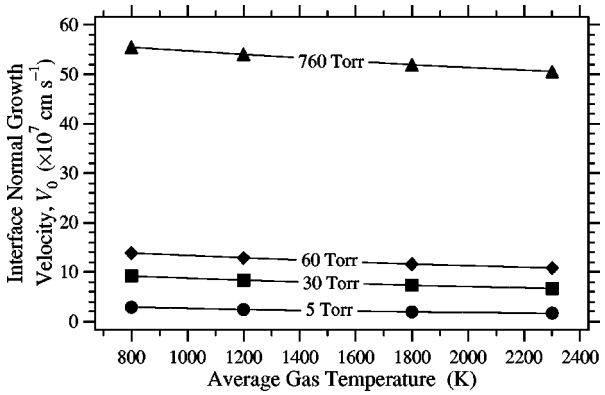


FIG. 8. The interface velocity, $V_0$, as a function of the effective gas temperature at system pressures of 5, 30, 60, and 760 Torr.

degree to which the interface is unstable. The critical velocity, $V_{\text{crit}}$, also increases with temperature at constant pressure, while the critical wave number, $\omega_c$, decreases with increasing temperature at constant pressure as may be observed in Figs. 6 and 7, respectively. The Landau coefficient, $a_1$, increases with increasing temperature, indicating increased stability to finite amplitude disturbances. As temperature is increased there is a commensurate increase in both linear and nonlinear stability because both $\beta$ and $\mathscr{D}_i$ increase; the effects of enhanced surface and gas-phase diffusion lead to increased stability to both finite and infinitesimal disturbances. Although morphological stability increases with increasing temperature, the interface growth velocity decreases at higher temperatures (Fig. 8) because the concentration of gaseous precursor species decreases at higher temperatures.

Since $a_0$ is positive for all temperatures, pressures, and gas compositions considered here, it may be concluded that diamond growth is morphologically unstable to infinitesimal disturbances. Diamond growth is also unstable to finite amplitude disturbances at all pressures considered except at 760 Torr, although the instability to infinitesimal disturbances increases with increasing pressure. The linear and nonlinear stability analysis results confirm numerical calculations demonstrating that diamond film growth is morphologically unstable for all pressures and temperatures characteristic of diamond CVD.[9] Also, both linear and nonlinear analyses predict decreased instability with increasing temperature at constant pressure. When the temperature is held fixed, nonlinear analysis predicts decreased instability with increasing pressure and linear analysis predicts increased instability with increasing pressure.

Diamond interface instability may result in the formation of the ''fingerlike'' diamond morphology observed by Ravi,[36] in which the taller regions shadow the shorter regions. Once formed, these projections are enhanced because they experience higher temperatures and reactant concentrations; thus, these processes may be magnified with time, resulting in extremely complex diamond film morphologies. These mechanisms of competitive shadowing and nutrient starvation are a dramatic feature of high growth rate diamond synthesis.[36] In order to promote film uniformity and prevent thermal instabilities, it is proposed that higher reactor effec-

tive temperatures should be used. Such a categorical statement cannot be made about the reactor pressure because the nonlinear and linear analyses predict decreasing and increasing instability with increasing pressures, respectively.

## V. CONCLUSION

The analysis of the morphological stability of a solid–gas interface under diffusive transport of reactants to the interface is presented using linear and nonlinear perturbation theories. Unlike previous analyses, the model in this work includes all possible effects, including reactants' gas-phase diffusivity, surface diffusion, and surface kinetics. The Landau coefficient, or the nonlinear growth rate, is calculated using the direct method of undetermined coefficients. Perturbation theory is applied to investigate the stability of the diamond growth interface during diamond CVD. The linear stability analysis results obtained suggest increased instability of the diamond growth interface to infinitesimal disturbances in the interface, although the interface growth velocity increases at higher pressures and lower temperatures. There is a tradeoff between film uniformity and the diamond growth rate that can be achieved. Nonlinear analysis results suggest increased instability of the diamond interface to finite amplitude disturbances at lower reactor pressures and lower temperatures. It is found that the stabilizing effect of surface diffusion increases with increasing pressure, although the reactant gas-phase diffusivity decreases and this has an overall destabilizing effect on film uniformity. Increased stabilizing effects at higher pressures have a more pronounced effect on the nonlinear growth rate than the increased destabilizing effect, thereby making the growth interface more stable to finite disturbances at higher pressures. The converse is true for linear growth rate. The stabilizing effect of surface diffusion increases, and the destabilizing effect of mass transfer limitation decreases as the temperature increases. Therefore, the growth interface is more stable to both infinitesimal and finite disturbances as the temperature increases, although the growth velocity decreases at higher temperatures.

## ACKNOWLEDGMENTS

This work has been supported by the Gas/Surface Dynamics Section of the Naval Research Laboratory, Contract No. N00014-97-1-G020. Partial support has been supplied by Texas Instruments.

## APPENDIX: DEFINITIONS OF EXPRESSIONS

$$R_{20}=\frac{1}{\mathrm{Pe}}\left(\frac{\omega^2 C_{11}(0)\zeta_{11}}{2}+\frac{B\mathrm{Pe}^3\zeta_{11}^2}{4}-\frac{D^2 C_{11}(0)\zeta_{11}}{2}\right)+\xi\left(\frac{BPe^2\zeta_{11}^2}{4}+\frac{DC_{11}(0)\zeta_{11}}{2}\right)+\frac{\xi(A+B)\omega^2\zeta_{11}^2}{4},$$

$$S_{20}=\frac{\rho}{\mathrm{Pe}}\left(\frac{(\omega_{20}^*-\mu_{20}\omega_{20})R_{20}}{D_{20}}+\frac{DC_{11}(0)\,\delta\omega^2\zeta_{11}}{2}\right)+\frac{\rho}{\mathrm{Pe}}\left(-\frac{\omega^2 C_{11}(0)\zeta_{11}}{2}-\frac{B\mathrm{Pe}^3\zeta_{11}^2}{4}+\frac{D^2 C_{11}(0)\zeta_{11}}{2}\right)+\frac{\rho}{\mathrm{Pe}}\left(\frac{B\mathrm{Pe}^2\zeta_{11}^2\delta\omega^2}{2}\right),$$

$$N_{20}=2a_0-B\rho\mathrm{Pe}+\frac{(\omega_{20}^*-\mu_{20}\omega_{20})(1+\xi)B\rho}{D_{20}},$$

$$R_{22}=-\frac{1}{\mathrm{Pe}}\left(\frac{\zeta_{11}C_{11}(0)\omega^2}{2}-\frac{B\mathrm{Pe}^3\zeta_{11}^2}{4}+\frac{D^2 C_{11}(0)\zeta_{11}}{2}\right)+\xi\left(\frac{B\mathrm{Pe}^2\zeta_{11}^2}{4}+\frac{DC_{11}(0)\zeta_{11}}{2}-\frac{\omega^2\zeta_{11}^2(A+B)}{4}\right),$$

$$S_{22}=\frac{\rho}{\mathrm{Pe}}\left(\frac{\omega^2 C_{11}(0)\zeta_{11}}{2}-\frac{B\mathrm{Pe}^3\zeta_{11}^2}{4}+\frac{D^2 C_{11}(0)\zeta_{11}}{2}\right)+\frac{\rho}{\mathrm{Pe}}\left(\frac{B\mathrm{Pe}^2\,\delta\omega^2\zeta_{11}^2}{2}+\frac{DC_{11}(0)\,\delta\omega^2\zeta_{11}}{2}\right)+\frac{\rho}{\mathrm{Pe}}\left(\frac{R_{22}}{D_{22}}(\omega_{22}^*-\mu_{22}\omega_{22})\right),$$

$$N_{22}=2a_0-\rho B\mathrm{Pe}+16\beta\omega^4-\frac{4\rho}{\mathrm{Pe}}(A+B)\,\delta\omega^2+\frac{\rho Q_{22}}{D_{22}\mathrm{Pe}}(\omega_{22}^*-\mu_{22}\omega_{22}),$$

$$R_{31}=\frac{1}{\mathrm{Pe}}\left(\zeta_{11}C_{22}(0)\omega^2+\zeta_{22}C_{11}(0)\omega^2+\frac{\omega^2\zeta_{11}^2 DC_{11}(0)}{4}\right)+\frac{1}{\mathrm{Pe}}\left(B\mathrm{Pe}^3\zeta_{11}\zeta_{20}+\frac{B\mathrm{Pe}^3\zeta_{11}\zeta_{22}}{2}-\frac{B\mathrm{Pe}^4\zeta_{11}^3}{8}\right)+\frac{1}{\mathrm{Pe}}\left(-D^2C_{11}(0)\zeta_{20}-\frac{D^2C_{11}(0)\zeta_{22}}{2}\right)+\frac{1}{\mathrm{Pe}}\left(-\frac{3D^3C_{11}(0)\zeta_{11}^2}{8}-D^2C_{20}(0)\zeta_{11}-\frac{D^2C_{22}(0)\zeta_{11}}{2}\right)+\xi\left(B\mathrm{Pe}^2\zeta_{20}\zeta_{11}+\frac{B\mathrm{Pe}^2\zeta_{22}\zeta_{11}}{2}-\frac{B\mathrm{Pe}^3\zeta_{11}^3}{8}\right)+\xi\left(DC_{11}(0)\zeta_{20}+\frac{DC_{11}(0)\zeta_{22}}{2}+\frac{3D^2C_{11}(0)\zeta_{11}^2}{8}\right)+\xi\left(DC_{20}(0)\zeta_{11}+\frac{DC_{22}(0)\zeta_{11}}{2}\right)+\xi\left(-\frac{B\mathrm{Pe}\omega^2\zeta_{11}^3}{8}+\frac{\omega^2\zeta_{11}^2C_{11}(0)}{8}\right)+\xi\omega^2(A+B)\zeta_{11}\zeta_{22},$$

$$S_{31}=\frac{\rho}{\mathrm{Pe}}\left(\omega^2\zeta_{11}C_{22}(0)+\omega^2\zeta_{22}C_{11}(0)+\frac{\omega^2\zeta_{11}^2DC_{11}(0)}{4}\right)+\frac{\rho}{\mathrm{Pe}}\left(B\mathrm{Pe}^3\zeta_{11}\zeta_{20}+\frac{B\mathrm{Pe}^3\zeta_{11}\zeta_{22}}{2}-\frac{B\mathrm{Pe}^4\zeta_{11}^3}{8}\right)$$
$$+\frac{\rho}{\mathrm{Pe}}\left(-D^2C_{11}(0)\zeta_{20}-\frac{D^2C_{11}(0)\zeta_{22}}{2}\right)+\frac{\rho}{\mathrm{Pe}}\left(-\frac{3\zeta_{11}^2D^3C_{11}(0)}{8}-\zeta_{11}D^2C_{20}(0)-\frac{\zeta_{11}D^2C_{22}(0)}{2}-\frac{3B\mathrm{Pe}\delta\omega^4\zeta_{11}^3}{8}\right)$$
$$+\frac{\rho}{\mathrm{Pe}}\left(\frac{\delta\omega^4\zeta_{11}^2C_{11}(0)}{4}-B\mathrm{Pe}^2\delta\omega^2\zeta_{11}\zeta_{20}-\frac{B\mathrm{Pe}^2\delta\omega^2\zeta_{11}\zeta_{22}}{2}\right)+\frac{\rho}{\mathrm{Pe}}\left(\frac{3B\mathrm{Pe}^3\delta\omega^2\zeta_{11}^3}{8}-\frac{3\delta\omega^2\zeta_{11}D^2C_{11}(0)}{4}\right.$$
$$\left.-2B\mathrm{Pe}^2\delta\omega^2\zeta_{11}\zeta_{22}\right)-\frac{\rho}{\mathrm{Pe}}\left(\delta\omega^2\zeta_{11}DC_{20}(0)+\frac{\delta\omega^2\zeta_{11}DC_{22}(0)}{2}+2\delta\omega^2\zeta_{22}DC_{11}(0)\right)-\frac{3}{4}\beta\omega^6\zeta_{11}^3.$$


[1] H. J. Oh, S. W. Rhee, and I. S. Kang, J. Electrochem. Soc. **139**, 1714 (1992).
[2] S. Lichtner and J. Chen, Phys. Rev. Lett. **56**, 1396 (1986).
[3] G. S. Bales, A. C. Redfield, and A. Zangwill, Phys. Rev. Lett. **62**, 776 (1989).
[4] A. G. Dirks and H. J. Leamy, Thin Solid Films **158**, 313 (1988); **177**, 141 (1989).
[5] C. H. J. van den Brekel and A. K. Jansen, J. Cryst. Growth **43**, 364 (1978); **43**, 371 (1978).
[6] B. J. Palmer and R. G. Gordon, Thin Solid Films **158**, 313 (1988); **177**, 141 (1989).
[7] H. J. Viljoen, Thin Solid Films **236**, 281 (1993).
[8] H. J. Viljoen, J. J. Thiart, and V. Hlavacek, AIChE. J. **40**, 1032 (1994).
[9] P. Mahalingam and D. S. Dandy, Diamond Relat. Mater. **6**, 1759 (1997).
[10] W. W. Mullins and R. F. Sekerka, J. Appl. Phys. **34**, 323 (1963).
[11] W. W. Mullins and R. F. Sekerka, J. Appl. Phys. **35**, 444 (1964).
[12] R. F. Sekerka, J. Appl. Phys. **36**, 264 (1965).
[13] D. T. J. Hurle, J. Cryst. Growth **5**, 162 (1969).
[14] S. R. Coriell, D. T. J. Hurle, and R. F. Sekerka, J. Cryst. Growth **32**, 1 (1976).
[15] S. R. Coriell and R. F. Sekerka, *PhysicoChemical Hydrodynamics*, edited by D. T. J. Hurle and E. Jakeman (Pergamon, New York, 1981), Vol. 2, p. 281.
[16] D. T. J. Hurle, E. Jakeman, and A. A. Wheeler, J. Cryst. Growth **58**, 163 (1982).
[17] W. Kurz and D. J. Fisher, *Fundamentals of Solidification* (Trans. Tech., Aedermannsdorf, Switzerland, 1989), pp. 45–59.
[18] W. Kurz and R. Trivedi, Acta Metall. Mater. **38**, 1 (1990).
[19] S. H. Davis, in *Interactive Dynamics of Convection and Solidification* (Kluwer Academic, The Netherlands, 1992), pp. 31–52.
[20] S. R. Coriell, G. B. McFadden, and R. F. Sekerka, Annu. Rev. Mater. Sci. **15**, 119 (1985).
[21] D. J. Wollkind and L. A. Segel, Philos. Trans. R. Soc. London, Ser. A **268**, 351 (1970).
[22] J. T. Stuart, J. Fluid Mech. **9**, 353 (1960).
[23] J. Watson, J. Fluid Mech. **9**, 371 (1960).
[24] D. J. Wollkind, D. B. Oulton, and R. Sriranganathan, J. Phys. (Paris) **45**, 505 (1984).
[25] R. C. Bower, D. A. Kessler, J. Koplick, and H. Levine, Phys. Rev. A **29**, 1335 (1984).
[26] E. Ben Jacob, N. Goldenfeld, J. S. Langer, and G. Schön, Phys. Rev. A **29**, 330 (1984).
[27] G. B. McFadden and S. R. Coriell, Physica D **12**, 253 (1984).
[28] L. Unger, M. J. Bennet, and R. A. Brown, Phys. Rev. B **31**, 5923 (1985).
[29] L. Unger and R. A. Brown, Phys. Rev. B **31**, 5931 (1985).
[30] D. A. Kessler, J. Koplik, and H. Levine, Phys. Rev. A **30**, 2820 (1984).
[31] B. J. Palmer and R. G. Gorson, Thin Solid Films **158**, 313 (1988).
[32] N. Ohtake, H. Tokura, Y. Kuriyama, Y. Mashimo, and M. Yoshikawa, *Proceedings of the 1st International Symposium on Diamond and Diamond Like Films* (The Electrochemical Society, Pennington, New Jersey, 1989), p. 93.
[33] D. S. Dandy and M. E. Coltrin, J. Mater. Res. **10**, 1993 (1995).
[34] C. R. Reid, J. M. Prausnitz, and B. E. Poling, *The Properties of Gases and Liquids* (McGraw–Hill, New York, 1987).
[35] D. S. Dandy and J. Yun, J. Mater. Res. **12**, 1112 (1997).
[36] K. V. Ravi, J. Mater. Res. **7**, 384 (1992).
[37] D. G. Goodwin, J. Appl. Phys. **74**, 6888 (1993).
[38] D. G. Goodwin, J. Appl. Phys. **74**, 6895 (1993).
[39] M. Kardar, G. Parisi, and Y. C. Zhang, Phys. Rev. Lett. **56**, 889 (1986).
[40] W. W. Mullins, J. Appl. Phys. **28**, 333 (1957).
[41] K. Muller, J. Appl. Phys. **58**, 2573 (1985).
[42] J. J. D. Alexander, D. J. Wollkind, and R. F. Sekerka, J. Cryst. Growth **79**, 849 (1986).
[43] B. Caroli, C. Caroli, and B. Roulet, J. Phys. (Paris) **45**, 505 (1984).